

# X-ray variability and energy spectra from NGC5408 X-1 with *XMM-Newton*

M. D. Caballero-García<sup>1\*</sup>, T. M. Belloni<sup>1</sup>, A. Wolter<sup>2</sup>

<sup>1</sup> INAF-Osservatorio Astronomico di Brera, Via E. Bianchi 46, I-23807 Merate (LC), Italy

<sup>3</sup> INAF, Osservatorio Astronomico di Brera, via Brera 28, 20121 Milano, Italy

27 October 2021

## ABSTRACT

The notion of source states characterizing the X-ray emission from black hole binaries has revealed to be a very useful tool to disentangle the complex spectral and aperiodic phenomenology displayed by those classes of accreting objects. We seek to use the same tools for Ultra-Luminous X-ray (ULX) sources. We analyzed the data from the longest observations obtained from the ULX source in NGC 5408 (NGC 5408 X–1) taken by *XMM-Newton*. We performed a study of the timing and spectral properties of the source. In accordance with previous studies on similar sources, the intrinsic energy spectra of the source are well described by a cold accretion disc emission plus a curved high-energy emission component. We studied the broad-band noise variability of the source and found an anti-correlation between the root mean square variability in the 0.0001–0.2 Hz and intensity, similarly to what is observed in black-hole binaries during the hard states. We discuss the physical processes responsible for the X-ray features observed and suggest that NGC 5408 X–1 harbors a black hole accreting in an unusual bright hard-intermediate state.

**Key words:** black hole physics – X-rays: galaxies – X-rays: general

## 1 INTRODUCTION

Ultra-Luminous X-ray sources (ULXs) are point-like, off-nuclear, extra-galactic sources, with observed X-ray luminosities ( $L_X \geq 10^{39}$  erg s<sup>-1</sup>) higher than the Eddington luminosity for a stellar-mass black-hole ( $L_X \approx 10^{38}$  erg s<sup>-1</sup>). The true nature of these objects is still debated (Feng & Soria 2011; Fender & Belloni 2012) as there is still no unambiguous estimate for the mass of the compact object hosted in these systems. Assuming an isotropic emission, in order to avoid the violation of the Eddington limit, ULXs might be powered by accretion onto Intermediate Mass Black Holes (IMBHs) with masses in the range  $10^2 - 10^5 M_\odot$  (Colbert & Mushotzky 1999). It has been also suggested that ULXs appear very luminous due to a combination of moderately high mass, mild beaming and mild super-Eddington emission and that ULXs are an inhomogeneous population composed of more than one class (Colbert & Mushotzky 1999; Fabbiano & White 2006).

ULXs have been studied intensively over the last decades (see Feng & Soria 2011 for a review). As in the case of Black Hole Binaries (BHBs), some ULXs undergo spectral transitions from a *power-law state* to a *high-soft state* (see Belloni 2011 and reference therein for a description of the spectral states in BHBs). Nevertheless, the classification of ULXs into canonical BH states is much more uncertain than in BHBs (Makishima et al. 2007; Soria 2011). During the *power-law state* the spectra of ULXs show a

power-law spectral shape in the 3–8 keV spectral range, together with a high-energy turn-over at 6–7 keV, and a *soft excess* at low energies (e.g. Kaaret et al. 2006). This *soft excess* can be modelled by emission coming from the inner accretion disc and is characterized by a low inner disc temperature of  $\approx 0.2$  keV. This is expected if the black holes in these sources are indeed IMBHs (Miller et al. 2003, 2004). Other explanations for the *soft excess* imply a much smaller mass for the black hole in these sources, based on the idea that the accretion in the disc is not intrinsically standard, in contrast to the majority of BHBs (e.g. see Kajava & Poutanen 2009). Soria (2007) and Mapelli et al. (2009) suggest that at least some ULXs are consistent with black holes accreting at moderate rate with masses of  $\approx 50 - 100 M_\odot$ , as also supported by the analysis of N10 in the Cartwheel galaxy (Pizzolato et al. 2010).

The study of the timing properties of ULXs represent a promising way to confirm the associations/similarities with this class of sources and BHBs. Variability in accreting stellar-mass black holes is usually studied by means of the Fourier Analysis, which allows to produce Power Density Spectra (PDS) where several different components are usually observed. BHBs PDS are usually composed of broad components (in the form of red noise or band-limited noise) and narrow components (called Quasi Periodic Oscillations, QPOs). Although we still know little about the physical origin of these temporal features, their phenomenology has proved useful in defining and identifying accretion states (Belloni 2011). Heil et al. (2009) performed a study of the fast time variability on various ULXs and found that for some sources the fast

\* E-mail: mcaballe@brera.inaf.it

variability is suppressed for a reason which is currently unknown. Middleton et al. (2011) proposed that the fast variability is suppressed for the sources with small inclination angle where the wind does not enter the line-of-sight. Heil et al. (2009) also found that a group of ULXs (including NGC 5408 X–1) have similar variability and PDS as luminous BHBs and Active Galactic Nuclei (AGN) in the observed frequency band-pass ( $10^{-3} - 1$  Hz).

In this work we apply the Root Mean Square (rms)-Intensity Diagram (Muñoz-Darías, Motta & Belloni 2011), which has been proved to be useful to map states in BHBs (without the need of any spectral information). We perform timing and spectral studies, focusing on the evolution of the broad-band noise and on its dependence on the spectral properties of the source.

### 1.1 NGC 5408 X–1

The ULX in NGC 5408 X–1 was discovered with the *Einstein* observatory (Stewart et al., 1983) and its *soft excess* found with *ROSAT* (Fabian & Ward 1993). It is located in a close-by ( $D = 4.8$  Mpc, Karachentsev et al. 2002) small (size of  $2.2 \times 1.1$  kpc) starburst galaxy (Soria et al. 2006 and references therein) and at  $\approx 20$  arcsec from the centre of the galaxy. This ULX peaks in X-ray luminosity above  $L_X = 1 \times 10^{40}$  erg s $^{-1}$  and is relatively nearby. Grise et al. (2012) identified the optical counterpart possibly as a B0I supergiant star. Spherically-symmetric nebulae around NGC 5408 X–1 have been detected in radio and optical bands (Pakull & Mirioni 2003; Soria et al. 2006; Lang et al. 2007; Cseh et al. 2012). This might indicate the presence of strong winds from a high-mass accretion rate source. Strohmayer & Mushotzky (2009) found a QPO in its PDS centred at 0.01 Hz and inferred a mass for the black hole in the range of  $10^3 - 10^4 M_\odot$ . Nevertheless, Middleton et al. (2011) propose a much smaller mass ( $10^2 M_\odot$ ) in base of the QPO and the timing properties. They propose that NGC 5408 X–1 is accreting in a super-Eddington regime and that the QPO is analogous to the ultra-Low-Frequency QPO seen occasionally in a few BHBs. Recently, Dheeraj & Strohmayer (2012) studied the timing and spectral properties of NGC 5408 X–1 and have found that the QPO frequency is variable (within the frequency range 0.0001-0.19 Hz) and largely independent on the spectral parameters. They suggested that NGC 5408 X–1 is accreting in the *saturation regime* (increase of the QPO frequency with constant disc flux and power-law photon index) frequently observed in BHBs (Vignarca et al. 2003).

## 2 OBSERVATIONS AND DATA REDUCTION

In this work we considered the 6 long (120-130 ks) high-quality observations of NGC 5408 X–1 collected by the *XMM-Newton* satellite over 6 years (2006-2011). The EPIC camera was operating in the *Full Frame* mode and with the *Thin Filter* set (see Tab. 1). Some of the observations were affected by relatively high background rates (flaring). We removed these periods for the timing data analysis by inspecting the light curve of the source. For the spectral analysis, we applied the standard filtering of removing time periods with count-rates in the FOV higher than 0.4 cts/s (EPIC-pn only).

For the timing analysis, we filtered the EPIC pn+MOS event files, selecting only the best-calibrated events (pattern $\leq 4, 12$  for the pn and the MOS, respectively), and rejecting flagged events (i.e. keeping only flag= 0 events) from a circular region on the source (centre at coordinates RA = 14 h03 m19.6 s, Dec = –41 d22 m59.6 s; Gladstone et al. 2009) and radius 28 arcsec. The

radius chosen contains  $\approx 90\%$  of the source photons, which is an optimal choice for not including too much background<sup>1</sup>. No background subtraction was applied since the background contribution was found to be small. We payed particular attention to extract the list of photons not randomized in time. To this purpose, we used the tasks *epchain* for the pn and *emproc* (with *randomizetime=no*) for the MOS cameras, respectively.

For the spectral analysis we used only the EPIC pn camera, in order to avoid issues due to cross-calibration effects. Additionally, the EPIC pn camera has a higher effective area (i.e. double) than each one of the MOS cameras and has sufficient statistics for the spectral fitting. We filtered the event files, selecting only the best-calibrated events (pattern $\leq 4$  for the pn), and rejecting flagged events (flag= 0). We extracted the flux from a circular region on the source centred at the coordinates of the source and radius 28 arcsec. The background was extracted from an annular region (with inner and outer radius of 45, 75 arcsec, respectively) centred at the coordinates of the source (see Fig. 1). To check the dependence of our results on these choices we also performed a background subtraction from a region in the same chip of the source and far away from it and from the boundaries and have seen no difference in the results shown in this paper. We built response functions with the *Science Analysis System* (SAS) tasks *rmfgen* and *arfgen*. We fitted the background-subtracted spectra with standard spectral models in XSPEC 12.7.0 (Arnaud 1996). All errors quoted in this work are 68% ( $1\sigma$ ) confidence. The spectral fits were limited to the 0.3-10 keV range, where the calibration of the instruments is the best. The spectra were rebinned in order to have at least 25 counts for each background-subtracted spectral channel in order to perform the chi-squared fitting and to avoid oversampling of the intrinsic energy resolution by a factor larger than 3<sup>2</sup>.

## 3 ANALYSIS

### 3.1 Timing Analysis

We performed an analysis of the fast time variability of NGC 5408 X–1 separately in the 0.3-1 keV and 1-10 keV energy ranges. The (0.3-10 keV) EPIC count rate is (1.2 – 1.6) cts s $^{-1}$  on average. The time resolution of the instruments is 2.6 s (MOS) and 73.4 ms (pn).

For both analysis we took into account good time intervals (GTIs) similar to the ones by Dheeraj & Strohmayer (2012) (see their Fig. 1). We excluded the periods of high-background with the introduction of a minimum number of gaps in the light curve that might produce artificial noise in our study of the intrinsic variability from the source. These time periods (gaps) were excluded from the PDS generation. We used the GHATS package, developed under the IDL environment at INAF-OAB<sup>3</sup>, to produce the PDS from 2048 points in each light curve. The PDS were then averaged together for each observation. The pn+MOS light curve was binned at the lowest time resolution of the two (2.6 s). This yields a Nyquist frequency of = 0.19 Hz. The PDS were normalized according to Leahy et al. (1983). All of the PDS show low-frequency flat-topped noise.

<sup>1</sup> See Fig 7 from the *XMM-Newton Users Handbook*:

[http://xmm.esac.esa.int/external/xmm\\_user\\_support/documentation/uhb/XMM\\_UHB.pdf](http://xmm.esac.esa.int/external/xmm_user_support/documentation/uhb/XMM_UHB.pdf)

<sup>2</sup> As recommended in:

[http://xmm.esac.esa.int/sas/current/documentation/threads/PN\\_spectrum\\_thread.shtml](http://xmm.esac.esa.int/sas/current/documentation/threads/PN_spectrum_thread.shtml)

<sup>3</sup> [http://www.brera.inaf.it/utenti/belloni/GHATS\\_Package/Home.html](http://www.brera.inaf.it/utenti/belloni/GHATS_Package/Home.html)

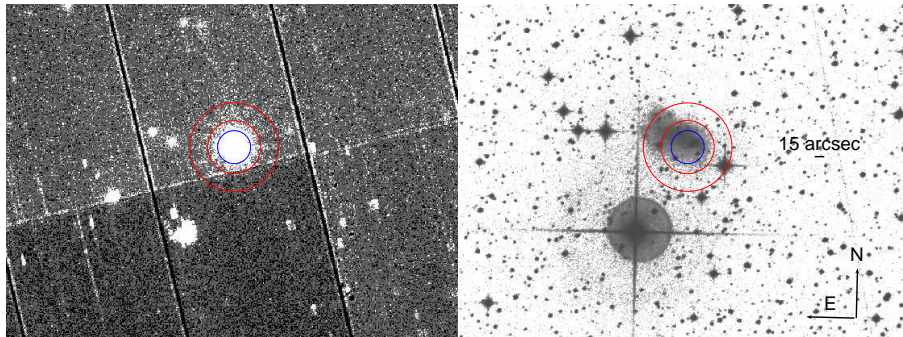


**Figure 1.** (12×12 arcmin) FOV of NGC 5408 X-1 with *XMM-Newton*/EPIC-pn (flag= 0 events; left) and (optical) STSCI-DSS I/II image (right). Regions for the spectral extraction of events of the source (circle/blue) and the background (annulus/red) are shown.

PDS fitting was carried out with the standard XSPEC fitting package by using a unit response. Fitting the (0.3-1 keV) PDS with a model constituted by a zero centred Lorentzian for the flat-topped noise plus a constant for the Poissonian noise results in mostly acceptable chi-square values only for the PDS of Obs. 4, 6 (see Tab. 2). In the case of Obs. 1, 2, 3 the fit statistics with this model is worse, i.e.  $\chi^2/\nu = 134/98, 120/98, 101/98$ , respectively. These observations and Obs. 5 (with a fit statistics of  $\chi^2/\nu = 88/98$  using the previous model) show positive residuals at  $\approx(0.002 - 0.02)$  Hz (see Tab. 2) that we fitted by adding a further Lorentzian component centred at those frequencies. This component changed the fits statistics by  $\Delta\chi^2 \leq 20$  for  $\Delta\nu = 3$  d.o.f., thus a  $\leq 3\sigma$  improvement. Although not significant for Obs. 2, 3, 5 we took into account these features, since they are broad and therefore affect substantially the measure of the rms, i.e. by (1 – 3)%.

The fit of the (1-10 keV) PDS with a model constituted by a zero centred Lorentzian for the flat-topped noise plus a constant for the Poissonian noise results in a poor description of the data. The fit statistics with this model is of  $\chi^2/\nu = 125/97, 116/98, 107/98, 130/98, 135/98, 149/98$  for Obs. 1-6, respectively. In all the observations there are positive residuals centred in the range of (0.01–0.04) Hz that we fitted by adding a further Lorentzian component centred at those frequencies. This component changed the fits statistics by  $\Delta\chi^2 \approx 33, 10, 16, 20, 50, 33.5$  for  $\Delta\nu = 3$  d.o.f., thus a (4.9, 2.9, 3.2, 3.9, 8.0, 4.2) $\sigma$  improvement for Obs. 1-6, respectively. This is a significant improvement for all the cases. We took into account this feature, since it is broad and therefore affects substantially our the measure of the rms, i.e. by  $\approx(1 - 4)\%$  for all the observations. In the case of Obs. 1, 4, 6 there is an excess at low frequencies and fitting it with a power-law yields a non-significant component ( $< 3\sigma$ ) for Obs. 1,6 that again we took into account, since the change in the fractional rms is of the order of (0.3 – 0.7)%. The photon index was unconstrained, so we fixed its value to 2, which is the asymptotic high-frequency slope of a Lorentzian. Additionally, the (1-10 keV) PDS of Obs. 2 shows positive residuals in the form of a peak centred at  $\nu_{\text{QPO}} \approx 0.01$  Hz, consistent with previous findings (Strohmayer & Mushotzky 2009). The detection of this peak is not significant ( $2.3\sigma$ , calculated as the value of the Lorentzian normalization divided by its  $1\sigma$  error). We did not include this component in our fits since it does not affect substantially the measure of the fractional rms ( $< 0.4\%$ ).

We calculated the fractional rms from the best fit model (integrated in the 0.0001-0.19 Hz band). This was found to be  $\approx 15\%$

and (30 – 50)% in the 0.3–1 keV and 1–10 keV energy ranges, respectively. The values obtained are reported in Tab. 2, together with the results from the fits and the count rates in the different energy ranges. We plot in Fig. 2 and 3 the broad-band PDS with the best-fit model. We notice that the integration of the rms from the data itself, without modeling, yields consistent values for the total fractional rms.

### 3.2 Spectral Analysis

Fig. 1 shows the galaxy area in X-rays and in the optical. The regions of the extraction of the flux from the source (circle) and the background (annulus) are also plotted. As can be seen, a small fraction of the inner region of the galaxy falls into the background extraction region. The (pn) count rate from the (annulus) background region is  $0.107 \pm 0.003$  cts  $\text{s}^{-1}$  in the (0.3-10 keV) energy range.

We started fitting the spectra with an absorbed power-law model, using the Tuebingen-Boulder ISM absorption model (tbabs in XSPEC) to account for the interstellar absorption ( $N_{\text{H}} = 7 \times 10^{20}$   $\text{cm}^{-2}$  in the direction to NGC 5408; Dickey & Lockman 1990). This parameter was set free to vary in order to account for intrinsic absorption. We fitted the spectra simultaneously, constraining the column density to be the same for all the spectra. With this model we obtained a bad description of the spectra  $\chi^2/\nu \gg 2$  (with  $\nu = 710$  d.o.f.), with positive residuals at  $\leq 2$  keV and high-energy curvature at  $\geq 5$  keV. The spectra are curved with a break at  $\approx 5 - 7$  keV, in agreement with what has been found in previous studies (see e.g. Stobbart et al. 2006; Gladstone et al. 2009; Caballero-Garcia & Fabian 2010). To account for the low-energy positive residuals we added a model constituted by an absorbed multicolor inner emission disc (diskbb or diskpn in XSPEC). The second is an extension of the first, including corrections for the temperature distribution near the black hole. To account for the high-energy residuals we added a cut-off, replacing the power-law component by an exponential rolloff (cutoffpl in XSPEC) model to fit the high-energy spectra. This model improved the fit substantially ( $\chi^2/\nu \approx 1.6$ , with  $\nu = 692$ ). We also tried by substituting the cutoff power-law by the more physical compTT model the latter with the temperature for the input photons equal to the inner disc temperature and obtained very similar quality of the fits ( $\chi^2/\nu \approx 1.6$ , with  $\nu = 692$ ). The resulting parameters are in agreement with previous studies (Gladstone et al. 2009; Middleton et al. 2011; Dheeraj & Strohmayer 2012).

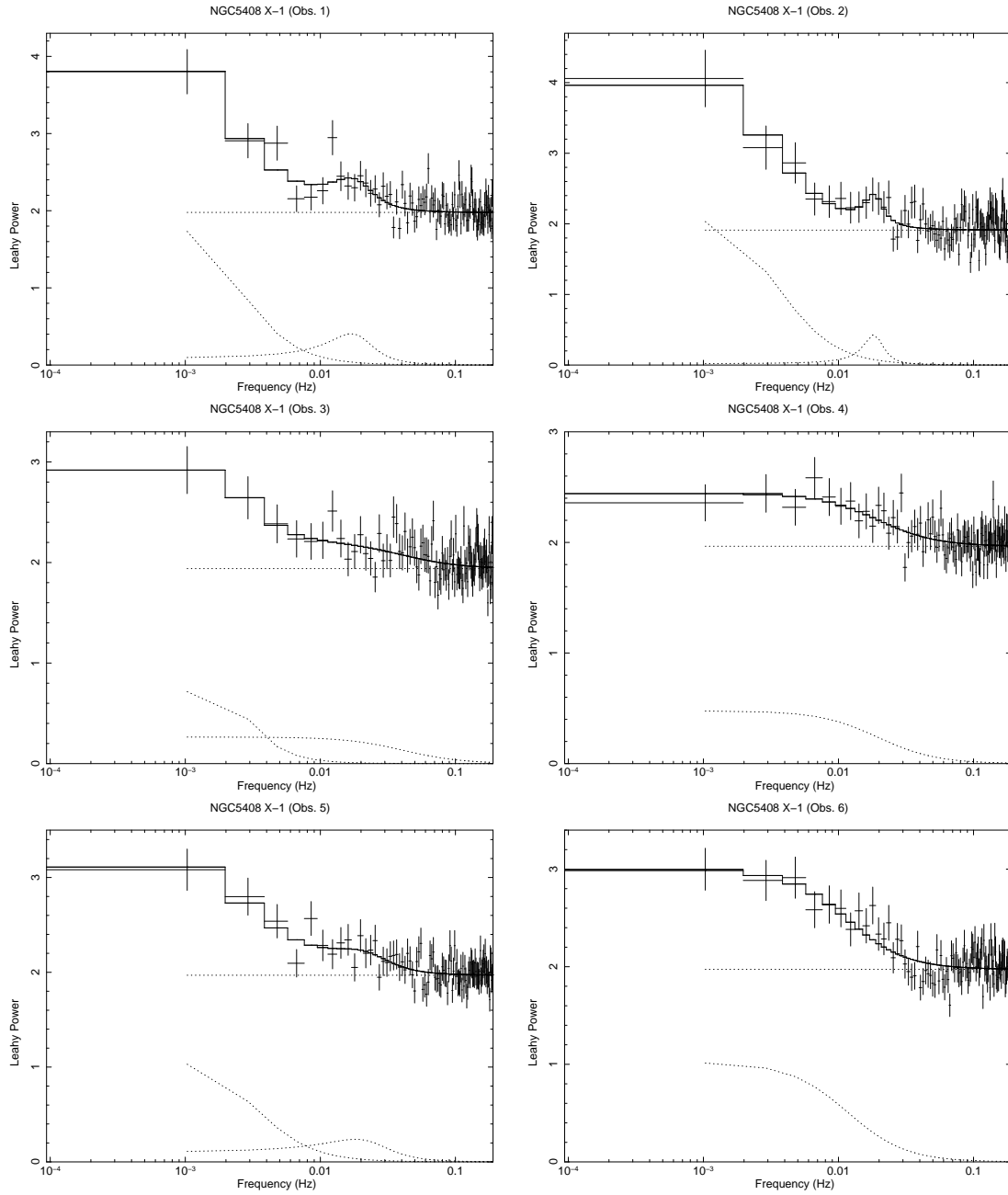


**Figure 2.** Power density spectra of the *XMM-Newton* EPIC/pn+MOS data in the energy and frequency range (0.3-1 keV) and 0.0001-0.19 Hz, respectively, during observations 1–6 (top-left to bottom-right) with the best fit model (solid line) and the model components (dotted line). The results of the fitting are shown in Tab. 2 and discussed in the text.

**Table 1.** Log of the observations.

	Obs. 1	Obs. 2	Obs. 3	Obs. 4	Obs. 5	Obs. 6
Date (dd/mm/yyyy)	13/01/2006	13/01/2008	17/07/2010	19/07/2010	26/01/2011	28/01/2011
Obs. ID	0302900101	0500750101	0653380201	0653380301	0653380401	0653380501
Exposure time (ks) <sup>1</sup>	130	114	127	129	119	124
Observation mode <sup>2</sup>	Full Frame	Full Frame	Full Frame	Full Frame	Full Frame	Full Frame

<sup>1</sup> The EPIC/pn exposure time.

<sup>2</sup> From the EPIC cameras.

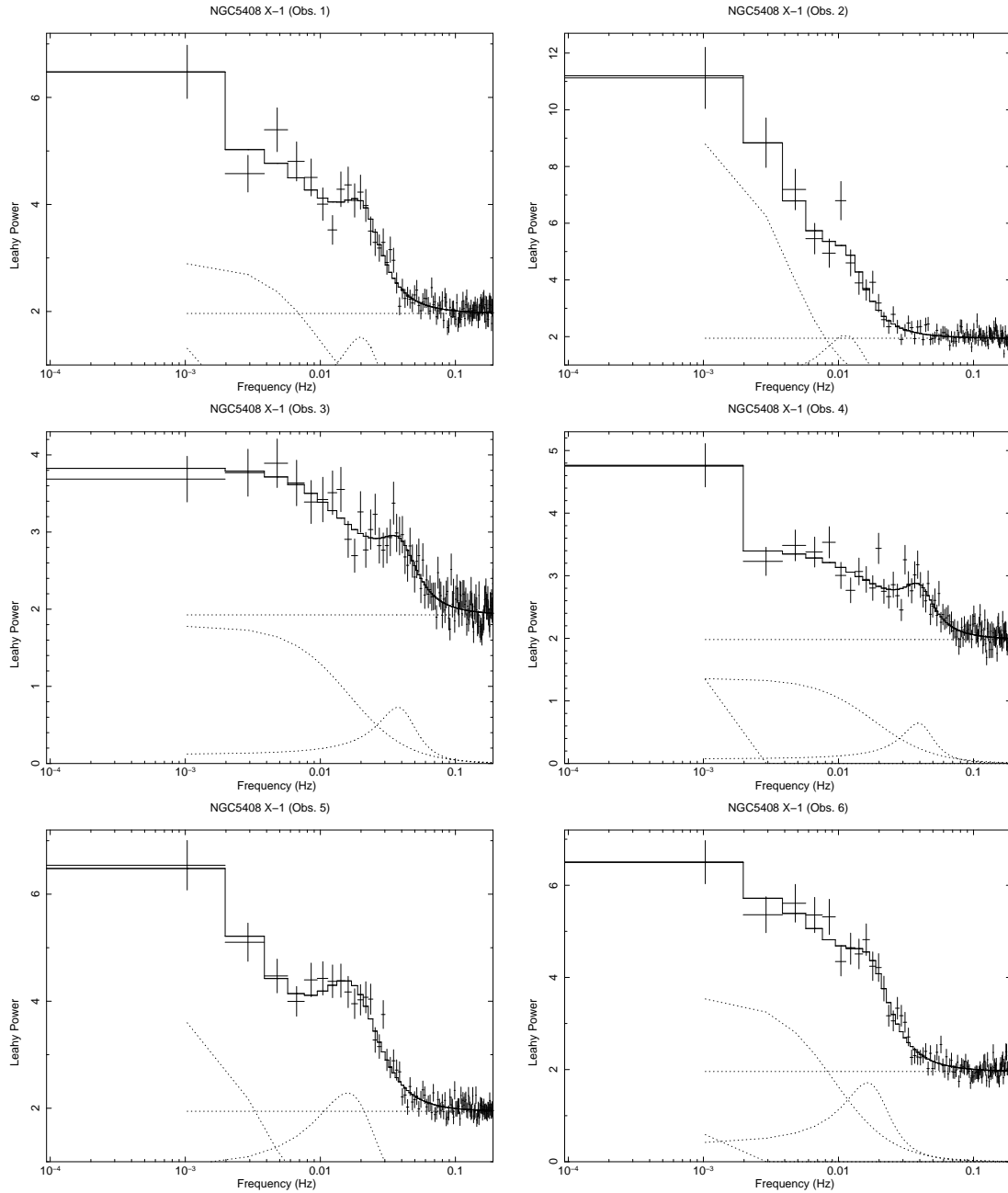


**Figure 3.** Power density spectra of the *XMM-Newton* EPIC/pn+MOS data in the energy and frequency range (1-10 keV) and 0.0001-0.19 Hz, respectively, during observations 1–6 (top-left to bottom-right) with the best fit model (solid line) and the model components (dotted line). The results of the fitting are shown in Tab. 2 and discussed in the text.

With the continuum model adopted (i.e. absorption, curved power-law and accretion disc) there are excesses at low energies (around 0.6 and 1 keV) that we attribute to the diffuse emission from the galaxy. To account for them we had to include two *apec* models (one was not enough) with temperatures of  $\approx 1, 0.1$  keV. We obtained a good fit ( $\chi^2/\nu \approx 1.0$ , with  $\nu = 688$  for all the spectral models used; see Tab. 3). The parameters of the *apec* models were constrained to be the same between the observations. We fixed the metal abundances to  $Z = 0.5 Z_{\odot}$  (sub-solar metallicities were found by Mendes de Oliveira et al. 2006). Nevertheless, the results do not significantly differ from the case of solar abundances and are insensitive of the sub-solar value adopted. The max-

imum temperature found for the diffuse X-ray component is by far too high compared to what is expected in regular non-starburst galaxies (i.e.  $kT_{\text{apec}} = 0.1 - 0.2$  keV). Indeed, NGC 5408 is a galaxy with a central starburst region (see Soria et al. 2006 and references therein). It has been seen (e.g. Buote & Fabian 1998; Warwick et al. 2007) that the highest X-ray quality data from starburst galaxies show plasmas in a multi-phase state, with two thermal diffuse emission components in their spectra, one cold and one hot ( $kT_{\text{apec}} = (0.1 - 0.6)$  keV,  $(0.8 - 1.0)$  keV), the hottest associated with the central starburst, in agreement with our findings.

The most X-ray luminous diffuse components are present in starburst galaxies (e.g. NGC 3256, NGC 253, M 82;

**Table 2.** Results from the timing analysis.

	Obs. 1	Obs. 2	Obs. 3	Obs. 4	Obs. 5	Obs. 6
<i>Soft</i> (0.3-1 keV) PDS						
Count rate <sup>3</sup> (cts s <sup>-1</sup> )	0.855±0.003	0.769±0.004	0.943±0.003	0.908±0.003	0.866±0.003	0.832±0.003
$\nu_V(1)$ (Hz)	0	0	0	0	0	0
FWHM (Hz)	0.005±0.002	0.007±0.002	0.08±0.04	0.039±0.010	0.006±0.002	0.023±0.004
Norm.	0.015±0.003	0.024±0.005	0.034±0.013	0.029±0.006	0.011±0.004	0.037±0.004
$\nu_V(2)$ (Hz)	0.017±0.002	0.018±0.003	0.0013±0.0010	–	0.018±0.011	–
FWHM (Hz)	0.018±0.005	0.007±0.005	0.004±0.003	–	0.03±0.02	–
Norm.	0.011±0.003	0.005±0.002	0.004±0.003	–	0.012±0.005	–
$\Gamma_{\text{poisson}}$	0	0	0	0	0	0
Norm. <sub>poisson</sub>	1.98±0.02	1.91±0.02	1.94±0.04	1.97±0.02	1.97±0.02	1.97±0.02
$\chi^2/\nu$	111/95	112/95	94/95	70/98	77/95	107/98
Fractional rms (%)	14.0±1.3	14.7±1.7	13.7±1.2	12.3±1.2	12.9±1.2	14.6±1.2
<i>Hard</i> (1-10 keV) PDS						
Count rate <sup>3</sup> (cts s <sup>-1</sup> )	0.429±0.002	0.426±0.003	0.574±0.003	0.552±0.002	0.500±0.002	0.490±0.002
$\nu_V(1)$ (Hz)	0	0	0	0	0	0
FWHM (Hz) <sup>2</sup>	0.020±0.005	0.008±0.002	0.033±0.007	0.037±0.010	0.006±0.002	0.018±0.005
Norm.	0.09±0.02	0.12±0.02	0.09±0.02	0.079±0.019	0.039±0.008	0.10±0.03
$\nu_V(2)$ (Hz)	0.020±0.002	0.011±0.002	0.038±0.003	0.039±0.002	0.016±0.002	0.016±0.002
FWHM (Hz) <sup>2</sup>	0.019±0.004	0.011±0.003	0.033±0.010	0.028±0.010	0.02±0.02	0.017±0.004
Norm.	0.046±0.014	0.038±0.013	0.037±0.014	0.028±0.013	0.089±0.010	0.047±0.017
$\Gamma$	2	–	–	2	–	2
Norm.	(2.4±1.1)×10 <sup>-7</sup>	–	–	(2.5±0.7)×10 <sup>-7</sup>	–	(1.1±1.0)×10 <sup>-7</sup>
$\Gamma_{\text{poisson}}$	0	0	0	0	0	0
Norm. <sub>poisson</sub>	1.96±0.02	1.94±0.02	1.93±0.03	1.98±0.02	1.94±0.02	1.96±0.02
Fractional rms (%)	44.4±1.0	45.6±1.4	36.0±0.9	33.9±0.8	41.8±0.8	42.7±0.9
$\chi^2/\nu$	87/94	101/95	91/95	93/94	78/95	114/94

Values for the count rate and characteristics of the noise (using the model<sup>1,2</sup>), separately in the 0.3-1 keV (i.e. *Soft PDS*: top) and in the 1-10 keV energy range (i.e. *Hard PDS*: bottom) for the six observations.

<sup>1</sup> Model used: A) lorentz+lorentz+powerlaw for the 0.3-1 keV energy range and B) lorentz+lorentz+powerlaw+powerlaw for the 1-10 keV energy range.

<sup>2</sup> Errors are 68% confidence errors.

<sup>3</sup> Background-subtracted count rate from the pn+MOS cameras.

Buote & Fabian 1998; Moran et al. 1999). For example, the total inferred luminosity of the diffuse plasma from the inner region (within a radius of 10.5 kpc in the plane of the galaxy) of the spiral star-forming galaxy M 101 is  $L_X(0.5 - 2 \text{ keV}) = 2.1 \times 10^{39} \text{ ergs}^{-1}$  (Warwick et al. 2007). The intrinsic (i.e. unabsorbed) luminosity of the diffuse plasma (i.e. from the *apex* model described above) from the inner (0.6 kpc) region of NGC 5408 is  $L_X(0.3 - 10 \text{ keV}) \approx 1 \times 10^{39} \text{ erg s}^{-1}$  (assuming a distance of 4.8 Mpc), thus  $\approx 10\%$  of the total (0.3-10 keV) intrinsic luminosity from the ULX. This value closely resembles the total luminosity of the diffuse thermal components of the dwarf starburst galaxy NGC 1569 ( $L_X(0.3 - 6 \text{ keV}) = 8.8 \times 10^{38} \text{ ergs}^{-1}$ ; Martin et al. 2002).

When using the *compTT* model to describe the high-energy component of the spectra (models C and D in Tab. 3), the obtained temperature of the electrons in the corona was  $kT_e \leq 5 \text{ keV}$  and the optical depth  $\tau = 3-6$ . In the phenomenological model with *cutoffpl* (model A and B in Tab. 3), the photon indices and the high-energy cut-off found are in the range 1.9–2.3 and 4–10 keV, respectively. The photon indices are very similar to those obtained from BHBs during the low/hard state ( $\Gamma = 1.7-2.0$ ,  $kT_{\text{in}} \approx 0.17 \text{ keV}$ , Reis et al. 2010) but the high-energy cut-off is much lower than those observed in BHBs ( $E = 60 - \geq 100 \text{ keV}$ ; Del Santo et al. 2009). The two high-energy spectral models provide the same sta-

tistical description to the data. The most relevant results of this spectral analysis and the derived unabsorbed fluxes are in Tab. 3 and in Fig. 4. The errors on the total flux (plus the flux from every individual component) were calculated using the *cflux* component in XSPEC.

### 3.3 Results

In Fig. 5 we show the light curve from the total flux (i.e. source plus emission from the diffuse component) and from the source, separated in its different components (disc and high-energy component – the last also called Comptonization component). Focusing on the light curve behaviour from the source we see that the disc component shows no significant variations (within  $2\sigma$  errors) in flux. On the other hand we see significant variations (at the  $3\sigma$  level with respect to the mean value) in the flux from the high-energy component. These variations are very similar to the variations from the total flux. Therefore, it looks like the variations of the total flux are due to variations of the high-energy component. Additionally, the broad-band noise in the 1-10 keV shows significant variations (at the  $3\sigma$  level with respect to the mean value). These two quantities (broad-band noise and total/high-energy component flux) appear to be anti-correlated, with a linear correlation coeffi-

**Table 3.** Results from the spectral analysis.

Spectral parameter <sup>1,2</sup>	Obs. 1	Obs. 2	Obs. 3	Obs. 4	Obs. 5	Obs. 6
A						
$N_H$ ( $\times 10^{22}$ ) ( $\text{cm}^{-2}$ )	0.113 $\pm$ 0.002	=	=	=	=	=
$kT_1$ (keV)	0.195 $\pm$ 0.003	=	=	=	=	=
$kT_2$ (keV)	1.000 $\pm$ 0.011	=	=	=	=	=
$F_{X,D}$ <sup>3</sup>	0.39 $\pm$ 0.02	=	=	=	=	=
$kT_{in}$ (keV)	0.156 $\pm$ 0.002	0.157 $\pm$ 0.004	0.161 $\pm$ 0.003	0.160 $\pm$ 0.003	0.160 $\pm$ 0.003	0.160 $\pm$ 0.004
$N_{disc}$	221 $\pm$ 21	179 $\pm$ 20	170 $\pm$ 21	148 $\pm$ 21	167 $\pm$ 20	136 $\pm$ 20
$\Gamma$	2.00 $\pm$ 0.02	1.89 $\pm$ 0.18	2.08 $\pm$ 0.10	2.27 $\pm$ 0.09	2.09 $\pm$ 0.11	2.32 $\pm$ 0.10
$E_c$ (keV)	4.4 $\pm$ 0.8	4.6 $\pm$ 1.2	5.6 $\pm$ 1.0	8.5 $\pm$ 1.9	5.7 $\pm$ 1.2	16 $\pm$ 6
$F_{disc}$ <sup>3</sup>	1.33 $\pm$ 0.05	1.13 $\pm$ 0.04	1.21 $\pm$ 0.05	1.01 $\pm$ 0.04	1.16 $\pm$ 0.05	0.93 $\pm$ 0.04
$F_{disc}(0.3 - 1 \text{ keV})$ <sup>3</sup>	1.26 $\pm$ 0.05	1.07 $\pm$ 0.04	1.14 $\pm$ 0.05	0.95 $\pm$ 0.04	1.10 $\pm$ 0.04	0.88 $\pm$ 0.03
$F_{disc}(1 - 10 \text{ keV})$ <sup>3</sup>	0.065 $\pm$ 0.003	0.058 $\pm$ 0.002	0.068 $\pm$ 0.003	0.055 $\pm$ 0.002	0.064 $\pm$ 0.003	0.051 $\pm$ 0.002
$L_{disc}(0.3 - 10 \text{ keV})$ <sup>6</sup> ( $\text{erg s}^{-1}$ )	(3.70 $\pm$ 0.14) $\times 10^{39}$	(3.14 $\pm$ 0.11) $\times 10^{39}$	(3.37 $\pm$ 0.14) $\times 10^{39}$	(2.81 $\pm$ 0.11) $\times 10^{39}$	(3.22 $\pm$ 0.14) $\times 10^{39}$	(2.59 $\pm$ 0.11) $\times 10^{39}$
$F_{pow}$ <sup>3</sup>	1.45 $\pm$ 0.06	1.40 $\pm$ 0.06	2.03 $\pm$ 0.08	2.13 $\pm$ 0.08	1.78 $\pm$ 0.07	1.96 $\pm$ 0.08
$F_{pow}(0.3 - 1 \text{ keV})$ <sup>3</sup>	0.72 $\pm$ 0.03	0.64 $\pm$ 0.03	1.01 $\pm$ 0.04	1.14 $\pm$ 0.05	0.89 $\pm$ 0.04	1.03 $\pm$ 0.04
$F_{pow}(1 - 10 \text{ keV})$ <sup>3</sup>	0.73 $\pm$ 0.03	0.76 $\pm$ 0.03	1.02 $\pm$ 0.04	0.99 $\pm$ 0.04	0.89 $\pm$ 0.04	0.93 $\pm$ 0.04
$F_{X,S}(0.3 - 1 \text{ keV})$ <sup>3</sup>	1.98 $\pm$ 0.08	1.71 $\pm$ 0.07	2.15 $\pm$ 0.09	2.10 $\pm$ 0.08	2.00 $\pm$ 0.08	1.90 $\pm$ 0.08
$F_{X,S}(1 - 10 \text{ keV})$ <sup>3</sup>	0.80 $\pm$ 0.03	0.82 $\pm$ 0.03	1.09 $\pm$ 0.04	1.04 $\pm$ 0.04	0.95 $\pm$ 0.04	0.98 $\pm$ 0.04
$F_{X,T}$ <sup>3</sup>	3.17 $\pm$ 0.13	2.92 $\pm$ 0.12	3.63 $\pm$ 0.14	3.53 $\pm$ 0.14	3.33 $\pm$ 0.13	3.28 $\pm$ 0.13
$\chi^2/\nu = 681/688$						
B						
$N_H$ ( $\times 10^{22}$ ) ( $\text{cm}^{-2}$ )	0.113 $\pm$ 0.002	=	=	=	=	=
$kT_1$ (keV)	0.195 $\pm$ 0.004	=	=	=	=	=
$kT_2$ (keV)	1.000 $\pm$ 0.011	=	=	=	=	=
$F_{X,D}$ <sup>3</sup>	0.39 $\pm$ 0.02	=	=	=	=	=
$kT_{max}$ (keV)	0.148 $\pm$ 0.002	0.150 $\pm$ 0.004	0.153 $\pm$ 0.003	0.152 $\pm$ 0.003	0.152 $\pm$ 0.003	0.152 $\pm$ 0.003
$N_{disc}$	(4.0 $\pm$ 0.4) $\times 10^{-3}$	(3.2 $\pm$ 0.4) $\times 10^{-3}$	(3.1 $\pm$ 0.4) $\times 10^{-3}$	(2.7 $\pm$ 0.4) $\times 10^{-3}$	(3.0 $\pm$ 0.4) $\times 10^{-3}$	(2.4 $\pm$ 0.4) $\times 10^{-3}$
$\Gamma$	2.01 $\pm$ 0.02	1.90 $\pm$ 0.18	2.08 $\pm$ 0.10	2.28 $\pm$ 0.09	2.10 $\pm$ 0.11	2.32 $\pm$ 0.10
$E_c$ (keV)	4.5 $\pm$ 0.7	4.6 $\pm$ 1.2	5.7 $\pm$ 1.0	8.6 $\pm$ 2.0	5.8 $\pm$ 1.2	16 $\pm$ 7
$F_{disc}$ <sup>3</sup>	1.32 $\pm$ 0.05	1.12 $\pm$ 0.04	1.21 $\pm$ 0.05	1.01 $\pm$ 0.04	1.16 $\pm$ 0.05	0.93 $\pm$ 0.04
$F_{disc}(0.3 - 1 \text{ keV})$ <sup>3</sup>	1.26 $\pm$ 0.05	1.07 $\pm$ 0.04	1.14 $\pm$ 0.05	0.95 $\pm$ 0.04	1.10 $\pm$ 0.04	0.88 $\pm$ 0.03
$F_{disc}(1 - 10 \text{ keV})$ <sup>3</sup>	0.064 $\pm$ 0.003	0.057 $\pm$ 0.002	0.067 $\pm$ 0.003	0.054 $\pm$ 0.002	0.063 $\pm$ 0.002	0.051 $\pm$ 0.002
$L_{disc}(0.3 - 10 \text{ keV})$ <sup>6</sup> ( $\text{erg s}^{-1}$ )	(3.67 $\pm$ 0.14) $\times 10^{39}$	(3.12 $\pm$ 0.11) $\times 10^{39}$	(3.37 $\pm$ 0.14) $\times 10^{39}$	(2.81 $\pm$ 0.11) $\times 10^{39}$	(3.23 $\pm$ 0.14) $\times 10^{39}$	(2.59 $\pm$ 0.11) $\times 10^{39}$
$F_{pow}$ <sup>3</sup>	1.46 $\pm$ 0.06	1.41 $\pm$ 0.06	2.04 $\pm$ 0.08	2.14 $\pm$ 0.08	1.79 $\pm$ 0.07	1.97 $\pm$ 0.08
$F_{pow}(0.3 - 1 \text{ keV})$ <sup>3</sup>	0.73 $\pm$ 0.03	0.65 $\pm$ 0.03	1.02 $\pm$ 0.04	1.15 $\pm$ 0.05	0.90 $\pm$ 0.04	1.03 $\pm$ 0.04
$F_{pow}(1 - 10 \text{ keV})$ <sup>3</sup>	0.73 $\pm$ 0.03	0.76 $\pm$ 0.03	1.02 $\pm$ 0.04	0.99 $\pm$ 0.04	0.89 $\pm$ 0.04	0.93 $\pm$ 0.04
$F_{X,S}(0.3 - 1 \text{ keV})$ <sup>3</sup>	1.98 $\pm$ 0.08	1.71 $\pm$ 0.07	2.16 $\pm$ 0.09	2.10 $\pm$ 0.08	2.00 $\pm$ 0.08	1.90 $\pm$ 0.08
$F_{X,S}(1 - 10 \text{ keV})$ <sup>3</sup>	0.80 $\pm$ 0.03	0.82 $\pm$ 0.03	1.09 $\pm$ 0.04	1.04 $\pm$ 0.04	0.95 $\pm$ 0.04	0.98 $\pm$ 0.04
$F_{X,T}$ <sup>3</sup>	3.17 $\pm$ 0.13	2.93 $\pm$ 0.12	3.63 $\pm$ 0.14	3.54 $\pm$ 0.14	3.34 $\pm$ 0.13	3.29 $\pm$ 0.13
$\chi^2/\nu = 681/688$						

<sup>1</sup> The spectral models used are: A) `tbabs(apec+apec+diskbb+cutoffpl)`, B) `tbabs(apec+apec+diskpn+cutoffpl)`, C) `tbabs(apec+apec+diskbb+comptt)` and D) `tbabs(apec+apec+diskpn+comptt)`.

<sup>2</sup> Errors are 68% confidence errors.

<sup>3</sup> Unabsorbed flux in the 0.3–10 keV energy range, in units of  $\times 10^{-12} \text{ergs}^{-1} \text{cm}^{-2}$ .

Description of the parameters:

1) Total column density  $N_H$ ; 2) temperatures from the emission components describing the diffuse emission from the galaxy ( $kT_1$  and  $kT_2$ ); 3) unabsorbed flux from the diffuse emission of the galaxy and from the source ( $F_{X,D}$ ,  $F_{X,S}$ ); 4) temperature from the inner accretion disc ( $kT_{in}$  and  $kT_{max}$  for the `diskbb` and `diskpn` components, respectively) and normalization from the disc component ( $N_{disc}$ ); 5) temperature of the electrons and opacity of the corona ( $kT_e, \tau$ ) from the `comptt` model component; 6) power-law photon index ( $\Gamma$ ) and e-folding energy of the exponential rolloff ( $E_c$ ) for the `cutoffpl` model component; 7) unabsorbed flux of the disc emission component ( $F_{disc}$ ) and corresponding luminosity ( $L_{disc}$ ; assuming a distance of 4.8 Mpc) in the 0.3–10 keV energy range; 8) unabsorbed flux from the high-energy emission component ( $F_{pow}$  and  $F_{comptt}$ ; for the `cutoffpl` or `comptt` model components, respectively) in the 0.3–10 keV energy range; and 9) unabsorbed total flux (source plus diffuse emission from the galaxy) in the 0.3–10 keV energy range ( $F_{X,T}$ ).

**Table 3.** (Continued.)

Spectral parameter <sup>1,2</sup>	Obs. 1	Obs. 2	Obs. 3	Obs. 4	Obs. 5	Obs. 6
C						
$N_H$ ( $\times 10^{22}$ ) ( $\text{cm}^{-2}$ )	0.108 $\pm$ 0.002	=	=	=	=	=
$kT_1$ (keV)	0.195 $\pm$ 0.003	=	=	=	=	=
$kT_2$ (keV)	1.001 $\pm$ 0.011	=	=	=	=	=
$F_{X,D}$ <sup>3</sup>	0.37 $\pm$ 0.02	=	=	=	=	=
$kT_{in}$ (keV)	0.140 $\pm$ 0.002	0.140 $\pm$ 0.004	0.140 $\pm$ 0.003	0.137 $\pm$ 0.004	0.140 $\pm$ 0.004	0.138 $\pm$ 0.004
$N_{disc}$	388 $\pm$ 9	330 $\pm$ 40	390 $\pm$ 30	410 $\pm$ 40	360 $\pm$ 30	360 $\pm$ 30
$kT_e$ (keV)	1.0 $^{+0.1}_{-1.0}$	1.0 $^{+0.13}_{-1.0}$	1.0 $^{+0.12}_{-1.0}$	1.0 $^{+0.3}_{-1.0}$	1.0 $^{+0.3}_{-1.0}$	4.2 $\pm$ 1.6
$\tau$	5.07 $\pm$ 0.11	5.2 $\pm$ 0.2	5.1 $\pm$ 0.2	4.8 $\pm$ 0.5	4.8 $\pm$ 0.5	3.5 $\pm$ 0.9
$F_{disc}$ <sup>3</sup>	1.37 $\pm$ 0.05	1.15 $\pm$ 0.05	1.34 $\pm$ 0.05	1.27 $\pm$ 0.05	1.28 $\pm$ 0.05	1.20 $\pm$ 0.05
$F_{disc}(0.3 - 1 \text{ keV})$ <sup>3</sup>	1.32 $\pm$ 0.05	1.11 $\pm$ 0.04	1.30 $\pm$ 0.05	1.23 $\pm$ 0.05	1.24 $\pm$ 0.05	1.16 $\pm$ 0.05
$F_{disc}(1 - 10 \text{ keV})$ <sup>3</sup>	0.044 $\pm$ 0.002	0.037 $\pm$ 0.002	0.043 $\pm$ 0.002	0.037 $\pm$ 0.002	0.041 $\pm$ 0.002	0.037 $\pm$ 0.002
$L_{disc}(0.3 - 10 \text{ keV})$ <sup>6</sup> ( $\text{erg s}^{-1}$ )	(3.81 $\pm$ 0.14) $\times 10^{39}$	(3.20 $\pm$ 0.14) $\times 10^{39}$	(3.73 $\pm$ 0.14) $\times 10^{39}$	(3.53 $\pm$ 0.14) $\times 10^{39}$	(3.56 $\pm$ 0.14) $\times 10^{39}$	(3.34 $\pm$ 0.14) $\times 10^{39}$
$F_{compTT}$ <sup>3</sup>	1.33 $\pm$ 0.05	1.36 $\pm$ 0.05	1.80 $\pm$ 0.07	1.75 $\pm$ 0.07	1.58 $\pm$ 0.06	1.59 $\pm$ 0.06
$F_{compTT}(0.3 - 1 \text{ keV})$ <sup>3</sup>	0.58 $\pm$ 0.02	0.55 $\pm$ 0.02	0.76 $\pm$ 0.03	0.76 $\pm$ 0.03	0.67 $\pm$ 0.03	0.65 $\pm$ 0.03
$F_{compTT}(1 - 10 \text{ keV})$ <sup>3</sup>	0.75 $\pm$ 0.03	0.81 $\pm$ 0.03	1.05 $\pm$ 0.04	1.00 $\pm$ 0.04	0.91 $\pm$ 0.04	0.94 $\pm$ 0.04
$F_{X,S}(0.3 - 1 \text{ keV})$ <sup>3</sup>	1.90 $\pm$ 0.08	1.65 $\pm$ 0.07	2.06 $\pm$ 0.08	2.00 $\pm$ 0.08	1.91 $\pm$ 0.08	1.81 $\pm$ 0.07
$F_{X,S}(1 - 10 \text{ keV})$ <sup>3</sup>	0.80 $\pm$ 0.03	0.85 $\pm$ 0.03	1.09 $\pm$ 0.04	1.03 $\pm$ 0.04	0.95 $\pm$ 0.04	0.97 $\pm$ 0.04
$F_{X,T}$ <sup>3</sup>	3.07 $\pm$ 0.12	2.87 $\pm$ 0.11	3.52 $\pm$ 0.14	3.39 $\pm$ 0.13	3.22 $\pm$ 0.13	3.16 $\pm$ 0.13
$\chi^2/\nu = 698/688$						
D						
$N_H$ ( $\times 10^{22}$ ) ( $\text{cm}^{-2}$ )	0.108 $\pm$ 0.004	=	=	=	=	=
$kT_1$ (keV)	0.194 $\pm$ 0.005	=	=	=	=	=
$kT_2$ (keV)	1.003 $\pm$ 0.011	=	=	=	=	=
$F_{X,D}$ <sup>3</sup>	0.36 $\pm$ 0.02	=	=	=	=	=
$kT_{max}$ (keV)	0.134 $\pm$ 0.003	0.134 $\pm$ 0.004	0.134 $\pm$ 0.003	0.131 $\pm$ 0.004	0.133 $\pm$ 0.002	0.133 $\pm$ 0.003
$N_{disc}$	(6.6 $\pm$ 0.4) $\times 10^{-3}$	(5.6 $\pm$ 0.6) $\times 10^{-3}$	(6.6 $\pm$ 0.6) $\times 10^{-3}$	(6.8 $\pm$ 0.7) $\times 10^{-3}$	(6.2 $\pm$ 0.5) $\times 10^{-3}$	(6.1 $\pm$ 0.6) $\times 10^{-3}$
$kT_e$ (keV)	1.0 $^{+0.2}_{-1.0}$	1.0 $^{+0.2}_{-1.0}$	1.0 $^{+0.2}_{-1.0}$	1.0 $^{+0.3}_{-1.0}$	1.0 $^{+0.3}_{-1.0}$	4.6 $\pm$ 1.9
$\tau$	5.0 $\pm$ 0.2	5.2 $\pm$ 0.2	5.1 $\pm$ 0.2	4.9 $\pm$ 0.4	4.8 $\pm$ 0.4	3.4 $\pm$ 1.0
$F_{disc}$ <sup>3</sup>	1.32 $\pm$ 0.05	1.11 $\pm$ 0.04	1.29 $\pm$ 0.05	1.21 $\pm$ 0.05	1.22 $\pm$ 0.05	1.14 $\pm$ 0.05
$F_{disc}(0.3 - 1 \text{ keV})$ <sup>3</sup>	1.28 $\pm$ 0.05	1.07 $\pm$ 0.04	1.25 $\pm$ 0.05	1.18 $\pm$ 0.05	1.18 $\pm$ 0.05	1.11 $\pm$ 0.04
$F_{disc}(1 - 10 \text{ keV})$ <sup>3</sup>	0.042 $\pm$ 0.002	0.036 $\pm$ 0.002	0.041 $\pm$ 0.002	0.036 $\pm$ 0.002	0.039 $\pm$ 0.002	0.035 $\pm$ 0.002
$L_{disc}(0.3 - 10 \text{ keV})$ <sup>6</sup> ( $\text{erg s}^{-1}$ )	(3.67 $\pm$ 0.14) $\times 10^{39}$	(3.09 $\pm$ 0.11) $\times 10^{39}$	(3.59 $\pm$ 0.14) $\times 10^{39}$	(3.37 $\pm$ 0.14) $\times 10^{39}$	(3.39 $\pm$ 0.14) $\times 10^{39}$	(3.17 $\pm$ 0.14) $\times 10^{39}$
$F_{compTT}$ <sup>3</sup>	1.36 $\pm$ 0.05	1.38 $\pm$ 0.05	1.85 $\pm$ 0.07	1.80 $\pm$ 0.07	1.62 $\pm$ 0.06	1.63 $\pm$ 0.07
$F_{compTT}(0.3 - 1 \text{ keV})$ <sup>3</sup>	0.61 $\pm$ 0.02	0.57 $\pm$ 0.02	0.80 $\pm$ 0.03	0.80 $\pm$ 0.03	0.71 $\pm$ 0.03	0.69 $\pm$ 0.03
$F_{compTT}(1 - 10 \text{ keV})$ <sup>3</sup>	0.75 $\pm$ 0.03	0.81 $\pm$ 0.03	1.05 $\pm$ 0.04	1.00 $\pm$ 0.04	0.91 $\pm$ 0.04	0.94 $\pm$ 0.04
$F_{X,S}(0.3 - 1 \text{ keV})$ <sup>3</sup>	1.89 $\pm$ 0.08	1.64 $\pm$ 0.07	2.04 $\pm$ 0.08	1.98 $\pm$ 0.08	1.89 $\pm$ 0.08	1.80 $\pm$ 0.07
$F_{X,S}(1 - 10 \text{ keV})$ <sup>3</sup>	0.80 $\pm$ 0.03	0.85 $\pm$ 0.03	1.09 $\pm$ 0.04	1.03 $\pm$ 0.04	0.95 $\pm$ 0.04	0.98 $\pm$ 0.04
$F_{X,T}$ <sup>3</sup>	3.04 $\pm$ 0.12	2.85 $\pm$ 0.11	3.49 $\pm$ 0.14	3.37 $\pm$ 0.13	3.20 $\pm$ 0.13	3.13 $\pm$ 0.12
$\chi^2/\nu = 697/688$						

cient of -0.87 (using the least-squares procedure). This corresponds to a chance probability of 0.6%. Also, the (1-10 keV) count rate is anti-correlated with the fractional rms, with a linear correlation coefficient of -0.93. This corresponds to a chance probability of 0.1% (see Fig. 6). Therefore, the anti-correlation is not connected to the specific spectral model used.

#### 4 DISCUSSION

In this paper we report on the timing and spectral analysis of the longest *XMM-Newton* observations of NGC 5408 X-1. The only significant ( $> 3\sigma$ ) spectral variation is the flux from the high-energy component (see Fig. 5). In the following we assume that the *soft excess* is physically a disc component, in order to compare with the case of BHBs. The variations in the flux from the disc component are less than  $2\sigma$  with respect to the mean value (where  $\sigma \approx 0.05 \times 10^{-12} \text{ erg s}^{-1}$  is the mean error from the flux values). Re-

garding the fast time variability from NGC 5408 X-1, the fractional rms in the 0.3–1 keV energy range does not significantly vary between the observations and is  $\approx (12 - 15)\%$  in the  $10^{-4} - 0.19 \text{ Hz}$  frequency range, in agreement with previous studies (Heil & Vaughan 2010; Middleton et al. 2011). On the contrary, the fractional rms in the 1–10 keV energy range is high (in agreement with the previous studies) and variable between the observations ( $\approx 30 - 50\%$ ). In the following our goal is to compare our findings with the case of BHBs.

Traditionally, the variability of BHBs has been associated to the high-energy emission component (e.g. Galeev et al. 1979; Poutanen & Fabian 1999; Churazov et al. 2001; Done et al. 2007). This is because, although strong variations in the luminosity of the disc component are seen on the long time-scales corresponding to transitions between the soft and the hard spectral states, the disc-dominated soft states show very little rapid variability (fractional rms  $\approx 1\%$ ; e.g. Belloni et al. 2005). In the low/hard state of BHBs the understanding of the origin of the variability has been limited



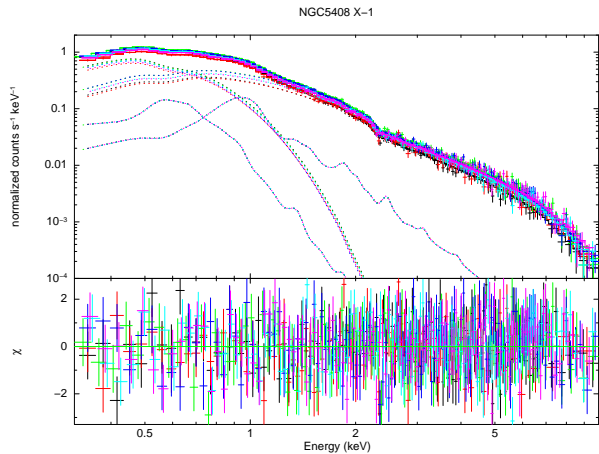


**Figure 4.** EPIC-pn *XMM-Newton* spectra (top) and chi-square residuals (bottom) of NGC5408 X-1 during observations 1-6 (in black, red, green, dark and light blue and magenta, respectively) fitted with the spectral model C.

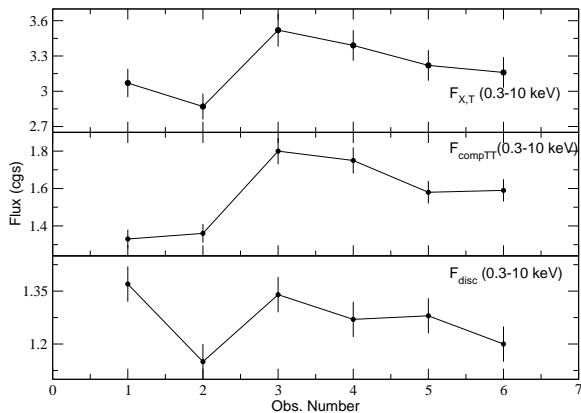


**Figure 5.** Unabsorbed fluxes (in the 0.3-10 keV energy range) versus the observation number. Total (with emission from the diffuse component), high-energy and disc component unabsorbed fluxes (top, middle and bottom, respectively). Values are reported in Tab. 3 and errors are 68% confidence. Spectral model C has been used in this plot to derive the fluxes.

by a lack of spectral coverage of the disc component, which emits at  $< 1$  keV, and so is not covered by the band-pass of detectors such as the *Proportional Counter Array* (PCA) on the *RXTE* satellite (2-60 keV). Nevertheless, a recent study of the X-ray variability in the low/hard state of BHBs has been performed with *XMM-Newton* (Wilkinson & Uttley 2009), who have found a disc component variability with a fractional rms of  $\approx 30-40\%$  for SWIFT J1753.5-0127 and GX 339-4 over long time-scales (2.7-270 s) when the source was in the low/hard state. From our work we see that in the case of NGC 5408 X-1 the 0.3-1 keV energy range is dominated by emission from the inner disc (contributing 60% of the total flux, with the high-energy component contributing 30% only). We have found that the fractional variability from NGC 5408 X-1 in the 0.3-1 keV energy range and  $10^{-4} - 0.19$  Hz frequency range is of  $\approx 15\%$ . This is less than what has been found in the *XMM-Newton* band-pass for BHBs. The difference might be due to the fact that both the disc and

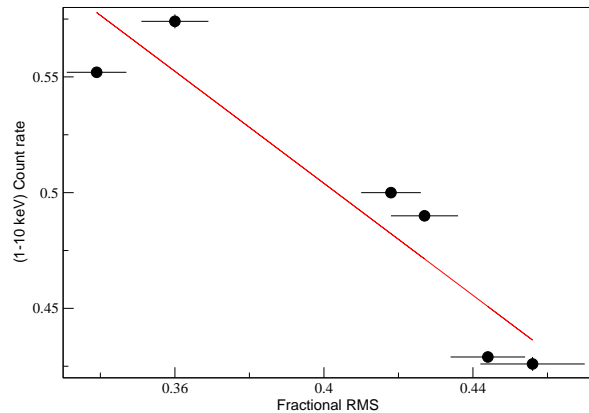


**Figure 6.** Count rate (in the 1-10 keV energy range) versus the fractional rms of the variability in the 1-10 keV energy range and 0.0001-0.19 Hz frequency range. Errors are 68% confidence. Poissonian errors on the count rate are smaller than the symbol.

the power-law components contribute differently to the 0.3-1 keV energy range in the case of NGC 5408 X-1 with respect to the case of BHBs, since the latter have hotter inner disc emission.

In contrast, rms of several tens per cent is seen in the low/hard spectral state of BHBs which are energetically dominated by the high-energy component emission in the *RXTE* band-pass (2-15 keV). We have found that in the case of NGC 5408 X-1 the 1-10 keV energy range is dominated by the high-energy emission component (contributing 90% of the total flux) and that little emission comes from the accretion disc in the 1-10 keV energy range (4%), similarly to what has been found in GX 339-4 in the 2-15 keV energy range during the low/hard state. This fact means that we can only use our results from the study of the fast variability of NGC 5408 X-1 in the 1-10 keV band for the comparison with the case of BHBs (i.e. measured with *RXTE*), since the contribution to the flux from the disc component are small in both cases. It is in this energy range (i.e. 1-10 keV) where we are measuring fractional rms variabilities similar to the high-energy component during the low/hard state of GX 339-4 (i.e. 30 - 40%).

From a detailed study of the variability of the BHB GX 339-4 with *RXTE* it has been seen that its variability decreases as its total flux (and the contribution from the disc component flux) increases. This has also seen to occur in a wider sample of BHBs using *RXTE* data only (Heil et al. 2012). We discovered that the (1-10 keV) count rate from NGC 5408 X-1 is anti-correlated with the fractional rms over long time-scales (years), similarly to the behaviour of the BHB GX 339-4 during the bright stage of the low/hard state measured with the *RXTE* satellite (Muñoz-Darias, Motta & Belloni 2011; hereafter called bright hard state). The relationship found by Muñoz-Darias, Motta & Belloni (2011) for GX 339-4 is valid over time-scales of weeks to months, thus shorter than in our case. Also, the noise in the PDS of NGC 5408 X-1 is in a lower frequency interval (0.0001-0.19 Hz) than GX 339-4 in the low/hard state (0.1-64 Hz frequency range; Muñoz-Darias, Motta & Belloni 2011). The fact that the characteristic time-scales of variability appear at lower frequency in the case of NGC 5408 X-1 with respect to GX 339-4 might be due to the higher mass of the BH and accretion rate in the former, as previously noticed to occur in a com-

parison in the case of BHBs with their higher mass analogs, i.e. the AGN (McHardy et al. 2006).

Previous studies revealed that a linear absolute rms versus flux positive correlation occurs on short time-scales (few ks) in NGC 5408 X–1 (Heil & Vaughan 2010). Contrary to our work, this result was found on short timescales where the PDS is restricted to being stationary. On the other hand, a recent study of the timing behaviour of BHBs (Heil et al. 2012) but using *RXTE* data ( $E \geq 2$  keV), has shown that the same rms-flux anti-correlation we have found here holds in the bright hard state of GX 339–4 (see their Fig. 4–5). This is in agreement with the results reported earlier by Muñoz-Darias, Motta & Belloni (2011). Both studies and our work use the non-stationary rms-flux on long timescales which samples changes to the whole PDS.

#### 4.1 On the Mass of the Black-Hole as found from previous studies

As described in Sec. 1, determining the mass from the BH in NGC 5408 X–1 has been the goal of several studies. However, there is still no consensus on whether it is an IMBH or a stellar-mass BH. Previous estimates from the timing properties (Strohmayer & Mushotzky 2009; Dheeraj & Strohmayer 2012) indicate a mass of  $M_{\text{BH}} \geq 1000 M_{\odot}$ , thus an IMBH, but others (Middleton et al. 2011) indicate a much smaller mass of  $M_{\text{BH}} \leq 100 M_{\odot}$ , thus a stellar-mass BH<sup>4</sup>. In the first case considered the accretion rate is sub-Eddington, whilst the latter case indicates (near or) super-Eddington accretion.

In the following we use the results obtained from the spectral analysis. The low inner disc temperatures found for some ULXs were interpreted as an evidence for the presence of IMBH (Miller et al. 2003, 2004). In the standard disc-black body model (i.e. Multi-Color Disc Blackbody or MCD; Makishima et al. 1986, 2000), which is a very poor approximation of the real standard accretion disc theory (Frank et al. 2002), the bolometric luminosity from the accretion disc is calculated as:

$$L_{\text{bol}} = 4\pi(R_{\text{in}}/\zeta)^2 \sigma (T_{\text{in}}/\kappa)^4 \quad (1)$$

Here  $\kappa \approx 1.7$  (Shimura et al. 1995) is the ratio of the color temperature to the effective temperature, or “spectral hardening factor”, and  $\zeta$  is a correction factor taking into account the fact that  $T_{\text{in}}$  occurs at a radius somewhat larger than  $R_{\text{in}}$  (Kubota et al. 1998 give  $\zeta = 0.412$ ). The behaviour explained above is a viable explanation of the temperature-luminosity behaviour of most BHBs (see Done et al. 2007 and references therein). However, a recent spectral study of the spectral variability from a sample of ULXs, including NGC 5408 X–1 (Kajava & Poutanen 2009), has shown that the *soft excess* (i.e. the disc component fitted in the spectra) from NGC 5408 X–1 does not follow Eq. 1 but  $L_{\text{bol}} \propto T_{\text{in}}^{-3.5}$ . This in contrast to what is found for many BHBs and might indicate that the standard accretion disc theory is not a proper interpretation in the case of NGC 5408 X–1. This implies that the hypothesis on which the IMBH idea is relying (i.e. standard accretion disc theory and the presence of a cold disc) are not valid and it might indicate that the BH in NGC 5408 X–1 is not an IMBH.

Therefore, other inner disc configurations might be possible

in the case of NGC 5408 X–1. The large apparent luminosities in the case of ULXs can be explained by supercritical accretion (exceeding the Eddington luminosity) onto a stellar-mass BH. In a recent study (Poutanen et al. 2007) it has been proposed that at high accretion rates an outflow forms within the so-called spherization radius. For a face-on observer the luminosity is high because of geometrical beaming (King et al. 2001). Such an observer has a direct view of the inner hot accretion disc, which has a peak temperature  $T_{\text{max}} \approx 1$  keV in stellar-mass BHs. In this model the *soft excess* corresponds to the emission from the spherization radius. Therefore, having a stellar-mass BH implies the presence of a much hotter inner accretion disc (i.e. with temperatures higher than the *soft excess*), that would be observed in the spectrum if the inner disc inclination is low. This could be the responsible for the “Comptonization” component seen in the spectra from NGC 5408 X–1, that could be emission from the inner disc instead. Such a super-Eddington flow implies much lower values for the mass of the BH, i.e.  $M \approx 10 M_{\odot}$ , accreting at mildly super-Eddington rates ( $\dot{M}/\dot{M}_{\text{EDD}} \approx 10$ ). An alternative scenario has been proposed (Stobart et al. 2006; Roberts 2007; Soria 2007; Gladstone et al. 2009), in which the presence of a cold and optically thick corona is obscuring the inner region of the disc and in this case the MCD parameters cannot provide reliable estimates of the black hole mass. Again this scenario is compatible with a stellar-mass BH, i.e.  $M \approx 10 - 100 M_{\odot}$ . These models are consistent with the idea that there is a relatively stable component at soft energies diluting the variability as might be expected by a thermal disc (see Churazov et al. 2001) or optically thick photospheric component (Zdziarski et al. 2009, 2010).

#### 4.2 The accretion state

In this paper we have shown that the timing properties of NGC 5408 X–1 over long time-scales (years) show that the variability properties, in particular the rms, change and resemble those from the BHB GX 339–4 during the bright phase of the hard state. These properties are the presence of a high broad-band timing noise and an anti-correlation of the fractional rms versus the high-energy count rate.

In the case of BHBs the hard state is not only seen during low accretion rates. Indeed, high accretion levels have been reached in a few cases. In the case of GS 2023+338 and Cyg X–1; (Tanaka & Lewin 1995; Stern et al. 2001) quasi-Eddington luminosities have been observed during the hard state. NGC 5408 X–1 has similar properties to what is found in the BHB GX 339–4 during its bright hard state. Additionally, in the hard state of GX 339–4 the major spectral change is in the flux from the high-energy component (see Fig. 6 of Motta et al. 2009). This behaviour is again similar to what is seen in the case of NGC 5408 X–1 (Fig. 5).

Nevertheless, an identification of the accretion state with the low/hard state seen in BHBs can not be made. The spectral properties of NGC 5408 X–1 are like ULXs in the so called “power-law state” (Makishima et al. 2007; Soria 2011). As mentioned in Sec. 1, during the “power-law state” the spectra of ULXs show a power-law spectral shape in the 3–8 keV spectral range, together with a high-energy turn-over at 6–7 keV, and a *soft excess* at low energies (e.g. Kaaret et al. 2006). There might be a corona in the case of NGC 5408 X–1 (and other ULXs) that is much colder and thicker than in the case of BHBs. Alternatively, there could be an intense accretion wind that is producing both the spectrum shape and the variability observed. The different properties could be due simply

<sup>4</sup> It has to be noted here that in low metallicity environments BHs with masses up to 80–100  $M_{\text{BH}}$  can still be formed through direct stellar-collapse (Zampieri & Roberts 2009; Belczynski et al. 2010) and this is why we are referring to them as *stellar-mass* BHs.

because of a much higher Eddington ratio in the case of NGC 5408 X-1.

The absolute rms of NGC 5408 X-1 in our observations is compatible with being constant within  $1\sigma$  errors. This is not compatible with a low/hard state-like behaviour in BHBs (and GX 339-4 in particular), where the absolute rms increases with count rate (Muñoz-Darias, Motta & Belloni 2011). Alternatively, this behaviour is similar to what has been seen in GX 339-4 during the Hard Intermediate state, in particular at the point where its fractional variability is of 20% and where the presence of an accretion disc is detected for the first time (Muñoz-Darias, Motta & Belloni 2011). In this state the fractional rms decreases as the count rate increases, as we observe to occur in NGC 5408 X-1. The fact that the fractional rms is of the order of  $\approx 20\%$  in the case of GX 339-4 whilst in the case of NGC 5408 X-1 is of the order of  $\approx 40\%$  is not problematic, since it can be explained by the presence of a much colder accretion disc (see Sec. 4.1) for the ULX. This decreases the contribution of the accretion disc component in the 1-10 keV energy range and diminishes the effect of suppression of variability in this energy range for the ULX.

## ACKNOWLEDGMENTS

We thank the anonymous referee, S. E. Motta, L. Zampieri, R. Soria and J. C. Gladstone for discussions and insights. This work is based on observations made with *XMM-Newton*, an ESA science mission with instruments and contributions directly funded by ESA member states and the USA (NASA). MCG acknowledges support from INAF through a 2010 postdoctoral fellowship. TB and AW acknowledge support from grant ASI-INAF I/009/10/. The research leading to these results has received funding from the European Community's Seventh Framework Programme (FP7/2007-2013) under grant agreement number ITN 215212 Black Hole Universe. This research has made use of the General High-energy Aperiodic Timing Software (GHATS) package developed by T.M. Belloni at INAF - Osservatorio Astronomico di Brera.

## REFERENCES

- Arnaud, K. A., 1996, *Astronomical Data Analysis Software and Systems V*, ASP Conf. Ser., 101, 17
- Belczynski, K., Bulik, T., Fryer, C. L. et al., 2010, *ApJ*, 714, 1217
- Belloni, T., Homan, J., Casella, P. et al., 2005, *A&A*, 440, 207
- Belloni, T. M., 2011, *Astronomische Nachrichten*, 332, 324
- Buote, D. A. & Fabian, A. C., 1998, *MNRAS*, 296, 977
- Caballero-García, M. D. & Fabian, A. C., 2010, *MNRAS*, 402, 2559
- Churazov, E., Gilfanov, M. & Revnivtsev, M., 2001, *MNRAS*, 321, 759
- Colbert, E. J. M. & Mushotzky, R. F., 1999, *ApJ*, 519, 89
- Cseh, D., Corbel, S., Kaaret, P. et al., 2012, *ApJ*, 749, 17
- Del Santo, M., Belloni, T. M., Homan, J. et al., 2009, *MNRAS*, 392, 992
- Dheeraj, P. R. & Strohmayer, T. E. 2012, *ApJ*, 753, 139
- Dickey, J. M. & Lockman, F. J., 1990, *ARA&A*, 28, 215
- Done, C., Gierliński, M. & Kubota, A., 2007, *A&ARv*, 15, 1
- Fabbiano G. & White N. E., 2006, in Lewin W. H. G., van der Klis M., eds, *Compact Stellar X-ray Sources in Normal Galaxies*. Cambridge Univ. Press, Cambridge, p. 475
- Fabian, A. C. & Ward, M. J., 1993, *MNRAS*, 263L, 51
- Fender, R. & Belloni, T., 2012, *Science*, 337, 540
- Feng, H. & Soria, R., 2011, *NewAR*, 55, 166
- Frank, J., King, A. & Raine, D. J., *Accretion Power in Astrophysics*, by Juhan Frank and Andrew King and Derek Raine, pp. 398, Cambridge University Press
- Galeev, A. A., Rosner, R. & Vaiana, G. S., 1979, *ApJ*, 229, 318
- Gladstone, J. C., Roberts, T. P. & Done, C., 2009, *MNRAS*, 397, 1836
- Grisé, F., Kaaret, P., Corbel, S., et al., 2012, *ApJ*, 745, 123
- Heil, L. M., Vaughan, S. & Roberts, T. P., 2009, *MNRAS*, 397, 1061
- Heil, L. M. & Vaughan, S., 2010, *MNRAS*, 405, 86
- Heil, L. M., Vaughan, S. & Uttley, P., 2012, *MNRAS*, 422, 2620
- Kaaret, P., Simet, M. G., & Lang, C. C., 2006, *ApJ*, 646, 174
- Kajava, J. J. E. & Poutanen, J., 2009, *MNRAS*, 398, 1450
- Karachentsev I. D. et al., 2002, *A&A*, 404, 93
- King, A. R., Davies, M. B., Ward, M. J. et al., 2001, *ApJ*, 552L, 109
- Kubota, A., Tanaka, Y., Makishima, K., Ueda, Y., Dotani, T., Inoue, H. & Yamaoka, K., 1998, *PASJ*, 50, 667
- Lang, C. C., Kaaret, P., Corbel, S. & Mercer, A., 2007, *ApJ*, 666, 79
- Leahy D. A., Elsner R. F. & Weisskopf M. C., 1983, *ApJ*, 272, 256
- Makishima, K., Maejima, Y., Mitsuda, K. et al., 1986, *ApJ*, 308, 35
- Makishima, K., et al. 2000, *ApJ*, 535, 632
- Makishima, K., 2007, *IAUS* 238, 209
- Mapelli, M., Colpi, M. & Zampieri, L., 2009, *MNRAS*, 395L, 71
- Martin, C. L., Koblunicky, H. A. & Heckman, T. M., 2002, *ApJ*, 574, 663
- McHardy, I. M., Koerding, E., Knigge, C., Uttley, P. & Fender, R. P., 2006, *Natur*, 444, 730
- Mendes de Oliveira, C. L., Temporin, S., Cypriano, E. S. et al., 2006, *AJ*, 132, 570
- Middleton, M. J., Roberts, T. P., Done, C. & Jackson, F. E., 2011, *MNRAS*, 411, 644
- Miller, J. M., Fabbiano, G., Miller, M. C. & Fabian, A. C., 2003, *ApJ*, 585, 37
- Miller, J. M., Fabian, A. C. & Miller, M. C., 2004, *ApJ*, 607, 931
- Moran, E. C., Lehnert, M. D. & Helfand, D. J., 1999, *ApJ*, 526, 649
- Motta, S., Belloni, T. & Homan, J., 2009, *MNRAS*, 400, 1603
- Muñoz-Darias, T., Motta, S. & Belloni, T. M., 2011, *MNRAS*, 410, 679
- Pakull, M. W. & Mirioni, L., 2003, *RMxAC*, 15, 197
- Pizzolato, F., Wolter, A. & Trinchieri, G., 2010, *MNRAS*, 406, 1116
- Poutanen, J. & Fabian, A. C., 1999, *MNRAS*, 306L, 31
- Poutanen, J., Lipunova, G., Fabrika, S. et al., 2007, *MNRAS*, 377, 1187
- Reis, R. C., Fabian, A. C. & Miller, J. M., 2010, *MNRAS*, 402, 836
- Roberts, T. P. 2007, *Ap&SS*, 311, 203
- Shimura, T. & Takahara, F., 1995, *ApJ*, 445, 780
- Soria, R., Fender, R. P., Hannikainen, D. C. et al., 2006, *MNRAS*, 368, 1527
- Soria, R., 2007, *Ap&SS*, 311, 213
- Soria, R., 2011, *Astronomische Nachrichten*, 332, 330
- Stern, B. E., Beloborodov, A. M. & Poutanen, J., 2001, *ApJ*, 555, 829

- Stobart, A.-M., Roberts, T. P. & Wilms, J., 2006, MNRAS, 368, 397
- Strohmayer, T. E. & Mushotzky, R. F., 2009, ApJ, 703, 1386
- Tanaka, Y. & Lewin, W. H. G., 1995, in Lewin, W. H. G., van Paradijs J., van den Heuvel E., eds, X-Ray Binaries. Cambridge University Press, Cambridge, p. 126
- Vignarca, F., Migliari, S., Belloni, T. et al., 2009, A&A, 397, 729
- Warwick, R. S., Jenkins, L. P., Read, A. M. et al., 2007, MNRAS, 376, 1611
- Wilkinson, T. & Uttley, P., 2009, MNRAS, 397, 666
- Zampieri, L. & Roberts, T. P., 2009, MNRAS, 400, 677
- Zdziarski, A. A., Kawabata, R. & Mineshige, S., 2009, MNRAS, 399, 1633
- Zdziarski, A. A., Misra, R. & Gierliński, M., 2010, MNRAS, 402, 767